

Spatial-ORMLLM: Improve Spatial Relation Understanding in the Operating Room with Multimodal Large Language Model

Peiqi He^{1*}, Zhenhao Zhang^{2*†}, Yixiang Zhang¹, Xiongjun Zhao^{1‡}, Shaoliang Peng^{1‡}

¹Hunan University ²ShanghaiTech University

hepeiqi@hnu.edu.cn, zhangzh2024@shanghaitech.edu.cn, {zhangyixiang, zhaoxiongjun, slpeng}@hnu.edu.cn,

Abstract

Precise spatial modeling in the operating room (OR) is foundational to many clinical tasks, supporting intraoperative awareness, hazard avoidance, and surgical decision-making. While existing approaches leverage large-scale multimodal datasets for latent-space alignment to implicitly learn spatial relationships, they overlook the 3D capabilities of MLLMs. However, this approach raises two issues: 1) Operating rooms typically lack multiple video and audio sensors, making multimodal 3D data difficult to obtain; 2) Training solely on readily available 2D data fails to capture fine-grained details in complex scenes. To address this gap, we introduce **Spatial-ORMLLM**, the first large vision-language model for 3D spatial reasoning in operating rooms using only RGB modality to infer volumetric and semantic cues, enabling downstream medical tasks with detailed and holistic spatial context. Spatial-ORMLLM incorporates a Spatial-Enhanced Feature Fusion Block, which integrates 2D modality inputs with rich 3D spatial knowledge extracted by the estimation algorithm and then feeds the combined features into the visual tower. By employing a unified end-to-end MLLM framework, it combines powerful spatial features with textual features to deliver robust 3D scene reasoning without any additional expert annotations or sensor inputs. Experiments on multiple benchmark clinical datasets demonstrate that Spatial-ORMLLM achieves state-of-the-art performance and generalizes robustly to previously unseen surgical scenarios and downstream tasks.

Introduction

Modern operating rooms (ORs) are complex and high-stakes environments where precise spatial awareness is essential for ensuring surgical safety and operational efficiency. Both human clinicians and AI systems must interpret dynamic spatial relationships, such as the positions of personnel or the placement of surgical tools, to facilitate seamless coordination and mitigate potential risks. However, achieving robust 3D spatial reasoning in computer vision systems remains a significant challenge, particularly under the constrained sensing conditions frequently present in real-world clinical settings. In many hospitals, especially at the community or regional level, surgical data are typically limited to

*These authors contributed equally.

†Project Leader.

‡Corresponding Author

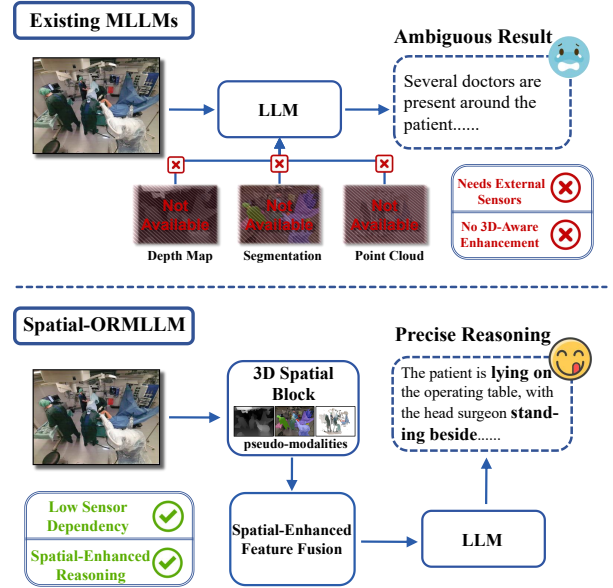


Figure 1: Comparison between existing MLLMs and the proposed Spatial-ORMLLM. Our model introduces spatial enhancements through pseudo-modalities and demonstrates more accurate spatial reasoning in OR scenes without requiring external sensors.

standard monocular RGB videos or images. Advanced sensing technologies such as depth cameras and densely annotated segmentation systems are rarely available due to financial constraints, infrastructure limitations, or concerns about disrupting clinical workflows. As a result, AI models often rely on sparse and weakly structured inputs that lack the geometric and semantic cues necessary for accurate scene understanding. As shown in Figure 1, these limitations are further exacerbated by the visual complexity of OR environments, which are often crowded, reflective, and prone to occlusions, factors that make spatial reasoning especially challenging for conventional vision-language models.

Recent advances in vision-language models have improved 2D visual understanding, particularly in image-text

alignment and grounded language generation. For instance, LLaVA (Liu et al. 2023) integrates a CLIP-based vision encoder with a large language model to enable image-conditioned dialogue and basic visual reasoning. Despite progress in multimodal interaction, these models often perform poorly on 3D understanding tasks due to the lack of 3D knowledge in large language models and the absence of explicit spatial reasoning capabilities.

Building on prior work, LLaVA-3D (Zhu et al. 2025) integrates 3D positional embeddings into a 2D LLM framework, enabling the incorporation of depth-related information into visual representations without requiring significant architectural modifications. While multi-view video inputs provide valuable spatial cues, they are often costly to obtain in medical environments and pose substantial challenges for domain adaptation. Depth maps estimated from general-purpose videos are typically noisy and imprecise, failing to meet the spatial accuracy demands of clinical applications. Furthermore, video-based inputs alone are limited in capturing fine-grained structural details, especially in complex environments such as operating rooms, where occlusions and dense object interactions are common. The absence of structured visual priors, such as panoptic segmentation, further constrains the model’s ability to parse and distinguish critical entities in these high-stakes settings accurately. In high-stakes environments like operating rooms, these limitations may lead to ambiguous or inaccurate interpretations of spatial configurations, which in turn can affect downstream decision-making. Addressing these challenges requires models that can reason about spatial relations more precisely, even when operating under modality-limited conditions.

To address these limitations, we propose Spatial-ORMLLM, the first large-scale vision-language model designed for 3D spatial understanding in clinical environments using only RGB inputs. The model incorporates three pseudo-modalities: depth maps, panoptic segmentation masks, and point clouds, which are treated as visual plugins and fused through a learnable integration module. This design enables Spatial-ORMLLM to jointly model geometric structure and semantic instance information from RGB images. As a result, the model supports fine-grained spatial reasoning, such as determining the location of surgical instruments relative to patients or identifying the positions of clinical staff, without relying on real three-dimensional sensors. This allows it to overcome key limitations of previous fusion-based approaches.

Our main contributions are summarized as follows:

- **Spatial-ORMLLM Framework:** We propose Spatial-ORMLLM, the first large vision-language model for 3D spatial reasoning in operating room environments, using only RGB modality and inferred geometric cues and enhanced via multimodal prompt guidance, designed to operate under modality-limited conditions.
- **Spatial-Enhanced Feature Fusion Block:** We design a multimodal feature fusion module that uses 2D modality and 3D pseudo-modalities as input. This enriched guidance enables the model to jointly capture geometric

structure and semantic context, supporting fine-grained reasoning in complex and cluttered OR scenes.

- **State-of-the-art Performance:** Our model achieves state-of-the-art performance on OR datasets using only RGB images, outperforming strong baselines across multiple metrics. Ablation studies confirm the complementary benefits of pseudo-modalities.

Related Work

Spatial Reasoning in VLMs

Recent advances in vision-language models (VLMs) have significantly pushed the boundary of image-grounded understanding. Models like Flamingo (Alayrac et al. 2022), BLIP-2 (Li et al. 2023), LLaVA (Liu et al. 2023), Spatial-LLM (Ma et al. 2025), Spatial-MLLM (Wu et al. 2025), and SpatialVLM (Chen et al. 2024a) integrate pre-trained vision encoders (e.g., CLIP (Radford et al. 2021)) with large language models and are adapted to instruction using synthetic datasets, often generated via GPT-4. These 2D large multimodal models (LMMs) demonstrate strong performance in image captioning, visual question answering, and multimodal dialogue. However, they primarily operate on RGB inputs and tend to lack explicit modeling of spatial structure and object relations, limiting their performance in geometry-aware reasoning tasks.

To address this limitation, recent efforts have introduced 3D spatial priors into multimodal LLMs. LLaVA-3D (Zhu et al. 2025) injects 3D positional encodings derived from point clouds into 2D vision tokens, allowing the model to predict 3D bounding boxes directly from image input. 3D-VisTA (Zhu et al. 2023) learns joint 2D-3D representations from RGB-D data to improve 3D-aware visual-language reasoning. 3D-LLaVA (Deng et al. 2025) uses point cloud prompts and a 3D-aware adapter to enhance spatial understanding in object-centric scenes, while VLM-3R (Fan et al. 2025) introduces instruction-aligned 3D reconstruction for reasoning from RGB. These works demonstrate that grounding language models in 3D geometry can boost spatial reasoning performance. However, most rely on dense supervision (e.g., LiDAR, RGB-D) or multi-view imagery during training—modalities that are rarely available in operating room settings.

Our approach differs in that we explore spatial reasoning under modality-limited conditions, using only RGB images. By leveraging pseudo-modalities, specifically inferred depth maps and segmentation masks, we enable geometric grounding without requiring real 3D sensors.

Medical Scene Understanding

Scene understanding in operating rooms has gained attention with the development of specialized medical datasets. 4D-OR (Özsoy et al. 2022) introduced a multi-view RGB-D dataset using Kinect sensors, annotated with 3D point clouds and scene graphs of surgical staff and tools. MM-OR (Özsoy et al. 2025) further scales this effort by providing multimodal recordings, including synchronized RGB-D video, audio, robot logs, and tracking data, along with panoptic segmentation and semantic graph annotations. These

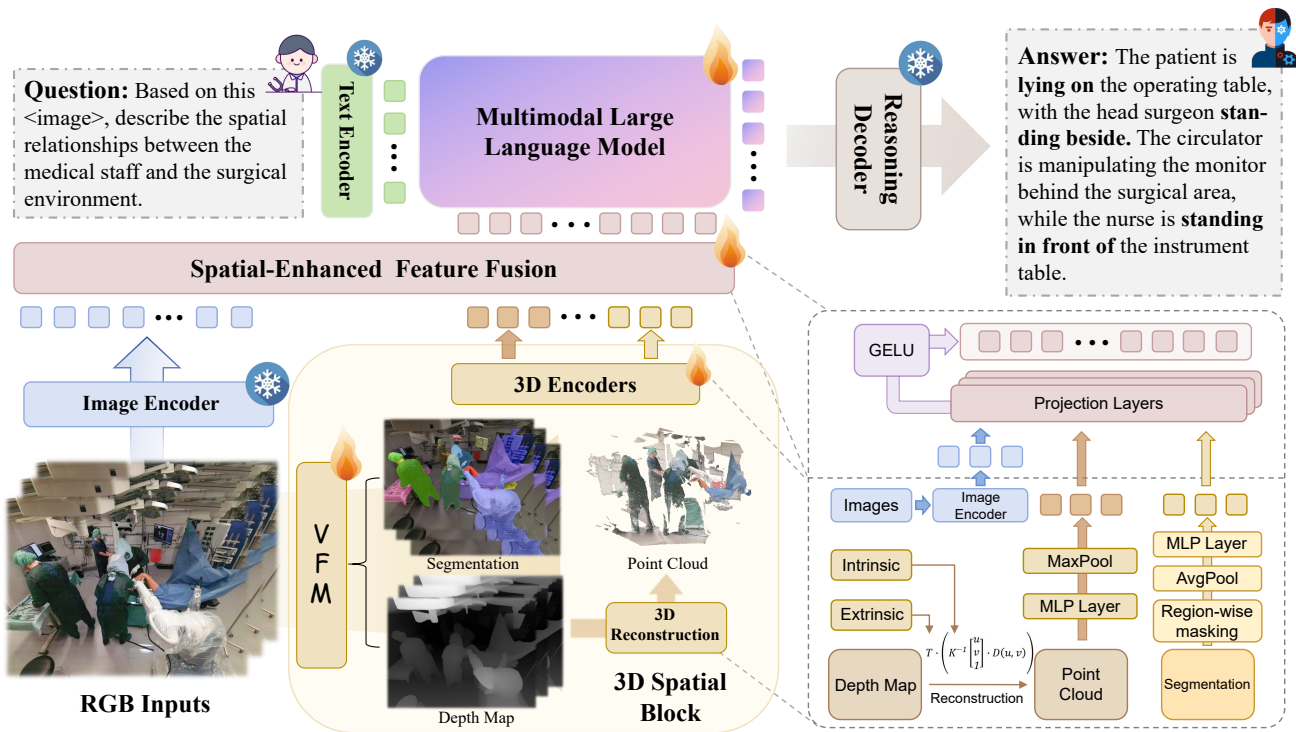


Figure 2: Architecture of the Spatial-ORMLLM framework. Starting from RGB images, our model generates three pseudo-modalities via a 3D Spatial Block. These are encoded into token sequences and fused with image tokens to form a unified multimodal input. The fused tokens are processed by a language model to perform spatial relation reasoning, enabling fine-grained understanding of surgical scenes using RGB-only inputs.

datasets enable fine-grained modeling of complex surgical workflows and serve as benchmarks for multimodal reasoning.

Existing models like MM2SG (Özsoy et al. 2025), ORacle (Özsoy et al. 2024), LABRAD-OR (Özsoy et al. 2023) and TriTemp-OR (Guo et al. 2024) leverage rich sensor modalities to generate scene graphs or spatial triplets. However, they often rely on multiview or depth input, making deployment in real-world ORs less practical. In contrast, our method focuses on enabling scene understanding from single RGB modality, which reflects the reality of many surgical data capture setups.

Beyond the OR domain, foundation models like SAM (Kirillov et al. 2023) and Depth Anything (Yang et al. 2024) have shown strong performance in segmentation and monocular depth estimation, respectively. Recent work has demonstrated that these models can be fine-tuned for surgical imagery to address blur, specular highlights, and occlusions common in OR videos (Lou et al. 2024; Kamtam et al. 2025). We build on this line by adapting these models to generate pseudo-modalities that enrich the vision-language model’s input and support spatial relation reasoning.

Method

Overview

As shown in Figure 2, Spatial-ORMLLM enhances RGB inputs with geometric and semantic cues. The 3D Spatial Block infers depth maps, panoptic segmentation, and point clouds from a single image $I \in \mathbf{R}^{3 \times H \times W}$. These pseudo-modalities are encoded into token representations and fused with image and prompt tokens. The unified sequence is passed to the LLM for spatial reasoning. Despite using only RGB input, the model achieves rich 3D understanding via internal inference and fusion.

3D Spatial Block

The 3D Spatial Block is responsible for extracting 3D geometry and semantics from a 2D image. It consists of two components: a visual feature modulator(VFM) to generate segmentation and depth map and a point cloud reconstructor.

3D Position Estimation Our depth estimation module is inspired by recent advances such as Depth Anything V2 (Yang et al. 2024), and is specifically adapted for medical scene understanding.

Given an input image I , the module predicts a dense depth map $D \in \mathbf{R}^{H \times W}$. The prediction process is defined as:

$$D = \mathcal{F}_d(I) = \text{Dec}(\text{Enc}(I)) \quad (1)$$

where $\text{Enc}(\cdot)$ is a transformer-based image encoder producing an intermediate feature map $F \in \mathbf{R}^{C \times H' \times W'}$, and $\text{Dec}(\cdot)$ is a lightweight upsampling decoder that outputs per-pixel depth. During training, we optimize the following loss:

$$\mathcal{L}_{\text{depth}} = \lambda_{\ell_1} \|D - D^*\|_1 + \lambda_{\text{grad}} \|\nabla D - \nabla D^*\|_1 \quad (2)$$

where D^* is the ground-truth depth captured by depth sensors, and ∇ denotes spatial gradients. This structure promotes both absolute accuracy and geometric smoothness in the predicted depth.

The resulting depth map D encodes rich spatial cues such as object contours, surface continuity, and relative distances that serve as pivotal input to the LLM for 3D spatial reasoning.

Complex Panoptic Segmentation Motivated by Segment Anything V2 (Kirillov et al. 2023), our segmentation module outputs a panoptic map S from RGB image I :

$$S = \text{SegDec}(\text{SegEnc}(I)) \in \{1, \dots, K\}^{H \times W} \quad (3)$$

where $\text{SegEnc}(\cdot)$ is a transformer-based encoder, and $\text{SegDec}(\cdot)$ is a lightweight mask decoder that assigns each pixel to one of K semantic categories.

Let $\hat{p}_{u,v,k} = \text{softmax}_k(S_{u,v,:})$ represent the predicted probability of category k at pixel (u, v) . We train this module using a combined cross-entropy and Dice loss:

$$\begin{aligned} \mathcal{L}_{\text{seg}} = & - \sum_{u,v,k} y_{u,v,k}^* \log \hat{p}_{u,v,k} \\ & + \lambda_{\text{Dice}} \sum_k (1 - \text{Dice}_k(\hat{p}, y^*)) \end{aligned} \quad (4)$$

where $y_{u,v,k}^*$ is the one-hot ground truth, and Dice_k computes the Dice coefficient for class k .

After segmentation, we encode the region-level panoptic output into a fixed-length feature representation. Given the panoptic map $S \in \{1, \dots, K\}^{H \times W}$, we define:

$$F_{\text{seg}} = [f_r]_{r=1}^R, \quad f_r = \phi(\text{Pool}(S == k_r)) \quad (5)$$

where $S == k_r$ performs region-wise masking to isolate pixels belonging to region r , $\text{Pool}(\cdot)$ is an average pooling layer that computes a summary over those pixels, k_r denotes its semantic class, and $\phi(\cdot)$ is a small MLP that encodes the pooled feature into a vector. The resulting set of features $F_{\text{seg}} = \{f_r\}$ captures semantic regions in a structured form.

These features serve as intermediate representations; they are not directly input to the LLM. Instead, they will later be projected into the shared token space and concatenated with RGB-based tokens.

The segmentation pipeline uses a transformer-based encoder and lightweight decoder, enhanced through domain-specific data augmentation and auxiliary semantic supervision. This design enables accurate localization and recognition of surgical and anatomical entities in the operating room environment.

Scene Point Cloud Reconstruction To inject explicit 3D structure, we reconstruct a partial point cloud P from the predicted depth. Given the camera intrinsics K and its pose T (extrinsics), each pixel (u, v) with depth value $D(u, v)$ can be back-projected into 3D space. We compute its 3D coordinates as:

$$P_{u,v} = T \cdot \left(K^{-1} \begin{bmatrix} u \\ v \\ 1 \end{bmatrix} \cdot D(u, v) \right) \quad (6)$$

where $K^{-1} \begin{bmatrix} u \\ v \\ 1 \end{bmatrix} \cdot D(u, v)$ gives the point in the camera coordinate frame and T transforms it into the world frame. Then, collecting all pixels yields a set of 3D points:

$$\mathcal{P} = \{P_{u,v} \mid (u, v) \in \Omega\}, \quad (7)$$

which constitutes a depth-based point cloud of the scene. This point cloud is essentially a geometric rendering of the image: it makes explicit the spatial arrangement of visible surfaces. Then, we encode it into a structured feature representation using a point cloud encoder. The encoder operates directly on the unordered point set \mathcal{P} , ensuring permutation invariance via shared multilayer perceptrons and a symmetric aggregation function (Qi et al. 2017). Formally, the encoding is defined as:

$$F_{\text{pc}} = \text{MaxPool}(\{\text{PCEnc}(p_i) \mid p_i \in \mathcal{P}\}) \quad (8)$$

where each point p_i is independently processed through the point cloud encoder, producing point-wise feature vectors. A global feature is obtained by applying a max-pooling operation across all points, capturing the global structure. The resulting feature $F_{\text{pc}} \in \mathbf{R}^C$ is then used as the basis for downstream tokenization.

This encoding step enables our model to capture essential 3D geometry such as relative distances, object extents, and free-space volumes, providing explicit spatial cues for downstream LLM reasoning.

Spatial-Enhanced Feature Fusion

A key innovation of Spatial-ORMLLM is the fusion of multimodal 3D features in the token space of the LLM. Instead of explicitly merging modalities early or requiring the LLM to query each modality separately, we project all modalities into a common embedding space and concatenate their token sequences as a unified input. This design enables the LLM to attend to and reason over a single sequence that jointly represents image patches, semantic masks, and 3D cues.

We begin by extracting visual tokens from the RGB image:

$$T_{\text{img}} = \mathcal{P}_{\text{img}}(\mathcal{E}_{\text{CLIP}}(I)) \quad (9)$$

where $\mathcal{E}_{\text{CLIP}}$ is the pretrained CLIP encoder and \mathcal{P}_{img} maps patch embeddings to d_{token} -dimensional tokens.

Next, we project the encoded segmentation and point cloud features:

$$T_{\text{seg}} = \mathcal{P}_{\text{seg}}(F_{\text{seg}}), \quad T_{\text{pc}} = \mathcal{P}_{\text{pc}}(F_{\text{pc}}) \quad (10)$$

where \mathcal{P}_{seg} and \mathcal{P}_{pc} are lightweight projection networks aligning these features into the same token space.

Model	Input-M	Used-M	R-L(%) \uparrow	M(%) \uparrow	C \uparrow	EM(%) \uparrow	AVG \uparrow
2D LMMs (Zero-shot)							
LLaVA-OV (Li et al. 2024)	RGB	RGB	46.6	38.8	60.1	28.7	43.6
Claude	RGB	RGB	–	45.7	88.2	–	–
Gemini	RGB	RGB	–	32.1	68.5	–	–
GPT-4V	RGB	RGB	–	36.9	60.6	–	–
OR-Domain Models							
ORacle (Özsoy et al. 2024)	RGB	RGB	53.1	44.0	87.1	55.8	60.0
MM2SG (Özsoy et al. 2025)	ALL*	ALL*	58.2	51.0	91.7	61.5	65.6
3D LMMs							
Scan2Cap (Chen et al. 2021)	PC	PC	–	33.6	56.4	–	–
LSenceLLM (Zhi et al. 2025)	PC	PC	54.1	47.1	80.6	63.2	61.3
3D-VisTA (Zhu et al. 2023)	PC	PC	48.4	39.1	70.0	25.8	45.8
LL3DA (Chen et al. 2024b)	PC	PC	51.2	45.2	77.0	60.8	58.6
3D-LLaVA (Deng et al. 2025)	PC	S + PC	56.3	50.0	90.9	50.2	61.9
3D-LLM (Hong et al. 2023)	RGB + PC	RGB + S + PC	47.0	41.1	73.3	56.5	54.5
LEO (Huang et al. 2024b)	RGB + PC	RGB + S + PC	56.9	49.8	88.5	61.2	64.1
Chat-Scene (Huang et al. 2024a)	RGB + PC	RGB + S + PC	55.6	52.2	88.8	57.7	63.6
LLaVA-3D (Zhu et al. 2025)	RGB	RGB + D	58.9	50.5	91.4	61.8	65.7
Spatial-ORMLLM (Ours)	RGB	RGB + D + S + PC	61.2	58.6	96.4	67.8	71.0

Table 1: Quantitative comparison of model performance on the spatial reasoning task on the combined OR dataset. **Input-M**: original input modalities, **Used-M**: all modalities involved in reasoning, including pseudo-modalities internally generated. Metrics: R-L = ROUGE-L, M = METEOR, C = CIDEr, EM = EM@1, AVG = average over all reported metrics. Modality abbreviations: RGB = RGB images/video, D = depth map, S = segmentation, PC = point cloud, **ALL*** = all modalities available in the original datasets(e.g., audio, logs).

Concretely, each modality (image, segmentation, and point cloud) is projected via a small feed-forward MLP network. Each projection head consists of two linear layers with a GELU activation in between, mapping input features into a shared token dimension d_{token} . These simple yet effective heads align multimodal representations into the LLM’s feature space.

We then concatenate all modality tokens along with prompt tokens T_{prompt} to form the final input sequence:

$$T_{\text{input}} = [T_{\text{img}}, T_{\text{seg}}, T_{\text{pc}}, T_{\text{prompt}}] \quad (11)$$

where each $T_i \in \mathbf{R}^{d_{\text{token}}}$.

This unified token sequence is fed into the LLM backbone \mathcal{F}_{LLM} , which processes these tokens together to produce

$$\text{Output} = \mathcal{F}_{\text{LLM}}(T_{\text{input}}; \theta_{\text{LLM}}) \quad (12)$$

where Output is the model’s answer or scene interpretation.

Our Spatial-Enhanced Feature Fusion module projects heterogeneous features into a unified token sequence, enabling joint attention-based reasoning within the LLM. All modalities share the same semantic space, allowing the LLM’s self-attention to operate across modalities. For example, a token corresponding to the operating table can attend to its co-located depth and segmentation tokens, achieving implicit spatial alignment without explicit geometric registration.

This token-level fusion offers key advantages. First, it supports implicit multimodal alignment through attention,

enabling the model to reason about spatial relationships such as identifying “the patient is lying on the operating table” by comparing depth and semantics. Second, the architecture is modular: new modalities (e.g., thermal or audio inputs) can be easily incorporated via the same projection-and-concatenation mechanism. Third, the sequence-based structure allows the LLM to perform context-aware, compositional reasoning over long multimodal inputs.

Experiments

Datasets

For our experiments, we collect and consolidate two operating room datasets, MM-OR (Özsoy et al. 2025) and 4D-OR (Özsoy et al. 2022), both of which record the full procedure of total knee replacement surgeries using multiple synchronized RGB-D cameras. The datasets are carefully annotated by medical experts to ensure high-quality supervision and semantic consistency. To better adapt the raw data to our model, we apply a weakly supervised preprocessing pipeline. The processed dataset includes multi-view RGB images, depth maps, panoptic segmentation masks, scene graphs, and scene descriptions. These multimodal inputs provide essential visual and semantic cues that support training and evaluation in perception, structured reasoning, and vision-language tasks. The final dataset includes 46,742 multimodal samples across diverse surgical scenes. We adopt a 60/20/20 train/val/test split. Further processing details are provided in the supplementary materials.

Training Strategy

We adopt a two-stage training procedure to progressively enhance the model’s reasoning capability and visual grounding in surgical environments.

Stage 1: Language Reasoning Adaptation. We freeze all vision-related components and train only the Vicuna-v1.5-7B (Zheng et al. 2023) LLM using medical-domain instruction-following data, enabling the model to acquire domain-specific reasoning skills related to surgical procedures and spatial understanding.

Stage 2: Visual Encoder and Projection Tuning. In the second stage, we freeze the LLM and fine-tune the visual encoders and modality-specific projection heads. This stage allows the visual components to adapt to the OR domain and align effectively with the language reasoning space established in Stage 1. We train the model on multimodal supervision datasets that contain paired RGB images, segmentation maps, depth-derived point clouds, and textual scene annotations.

This two-stage strategy ensures that the language model acquires strong domain knowledge before visual grounding is introduced, leading to more accurate multimodal reasoning in surgical scenes. We follow LLaVA-style training (Liu et al. 2023), optimizing language modeling and contrastive alignment losses to encourage coherent multimodal fusion. Details are provided in Appendix.

Evaluation Metrics

We adopt four standard metrics to evaluate response quality in scene reasoning:

- **ROUGE-L:** Evaluates the longest common subsequence between generated and reference texts, reflecting the overall sequence-level alignment and coverage.
- **METEOR:** Computes a harmonic mean of unigram precision and recall, integrating stemming and synonym matching. It offers better correlation with human judgment than BLEU in diverse reasoning tasks.
- **CIDEr:** Captures consensus between the generated output and multiple ground-truth answers using TF-IDF weighted n-gram similarity. It emphasizes informative and semantically relevant content, making it particularly suitable for scene-level descriptions.
- **EM@1:** Exact Match at Top-1 measures the proportion of outputs that exactly match at least one ground-truth answer. This strict metric is particularly important for factual correctness in structured question answering.

Main Result

We evaluate the proposed Spatial-ORMLLM on the combined surgical scene dataset, using a consistent evaluation split across all models. As summarized in Table 1, we compare our method against several state-of-the-art baselines, including domain-specific OR models, general 2D vision-language models, and general 3D multimodal models.

Spatial-ORMLLM achieves the highest overall performance across all key metrics on the OR spatial understanding benchmark. Our model consistently outperforms

or matches existing baselines, demonstrating its strong 3D spatial reasoning capabilities under modality-limited surgical scenarios. These results confirm the effectiveness of our approach and its potential for real-world surgical applications.

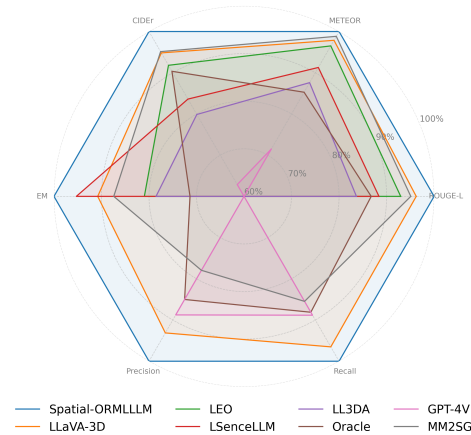


Figure 3: Quantitative evaluation of model performance on spatial reasoning and scene graph generation.

Model	P(%)↑	R(%)↑	F1(%)↑
GPT-4V	83.3	74.0	78.4
MM2SG	74.9	71.2	73.0
ORacle	81.7	73.4	77.3
LLaVA-3D	83.5	80.4	81.9
Ours	86.1	83.3	84.7

Table 2: Performance of different models on the OR scene graph generation task. Metrics include Precision (P), Recall (R), and F1-Score (F1).

Scene Graph Generation

To further evaluate the spatial reasoning capability of Spatial-ORMLLM, we adopt scene graph generation (SGG) as a downstream task. SGG is a well-established benchmark that assesses a model’s ability to identify semantic entities and their pairwise spatial relationships.

In our setting, we perform SGG using only RGB modality as input, without access to ground-truth depth, segmentation, or 3D annotations. We compare Spatial-ORMLLM against several representative models under this modality-limited setting. As shown in Table 2, our model achieves the highest performance across all metrics, surpassing state-of-the-art models.

These results confirm that Spatial-ORMLLM is capable of accurate structured scene understanding and fine-grained spatial relation modeling even under restricted input conditions.

Model Variant	R-L(%) \uparrow	M(%) \uparrow	C \uparrow	EM(%) \uparrow	AVG \uparrow	P(%) \uparrow	R(%) \uparrow	F1(%) \uparrow
w/o Point Cloud Reconstruction	57.9	51.2	89.9	64.6	65.9	82.3	79.5	80.9
w/o Panoptic Segmentation	58.4	51.3	91.9	61.2	65.7	80.9	78.3	79.6
w/o Depth Estimation	50.5	42.5	56.7	43.2	48.2	73.8	76.4	75.1
w/o Depth Est. & Panoptic Seg.	39.5	36.9	55.0	37.8	42.3	68.1	70.5	69.3
Spatial-ORMLLM (Full)	61.2	58.6	96.4	67.8	71.0	86.1	83.3	84.7

Table 3: Ablation study evaluating the impact of each pseudo-modality on spatial reasoning and scene graph generation. The first five metrics (ROUGE-L, METEOR, CIDEr, EM@1, Average) assess spatial reasoning, while the last three (Precision, Recall, F1-Score) evaluate scene graph generation quality.

Visualization

To better understand the spatial reasoning capability of our model, we provide qualitative and quantitative visualizations of Spatial-ORMLLM in both metric-based performance and scene-level spatial understanding, compared to existing baselines.

Figure 3 presents a comprehensive visualization of model performance across various evaluation metrics for spatial reasoning and scene graph generation. Our model outperforms prior baselines, confirming the benefit of pseudo-modal guidance and unified token-level fusion in enhancing spatial relation understanding under RGB-only conditions.

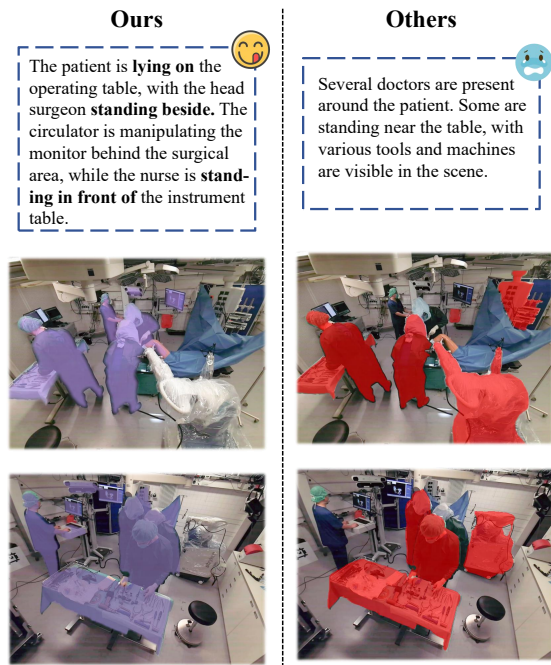


Figure 4: Qualitative comparison between Spatial-ORMLLM and baseline models.

We visualize the spatial reasoning capability of our model by comparing its output with those of baseline methods on representative surgical scenes. As shown in Figure 4, While baseline models often yield vague or partially correct scene

descriptions, our model demonstrates clearer attention to key spatial relationships. These results indicate that Spatial-ORMLLM is capable of attending to semantically important and spatially grounded regions, achieving a fine-grained interpretation of complex surgical environments.

Ablation Study

To investigate the contribution of each modality and component in our framework, we conduct a series of ablation studies on the combined surgical dataset. Specifically, we evaluate the following variants:

- **w/o Point Cloud Reconstruction:** Instead of reconstructing 3D point clouds from estimated depth, we directly treat the depth map as an additional 2D image input.
- **w/o Panoptic Segmentation:** We remove the panoptic segmentation branch and its corresponding token stream.
- **w/o Depth Estimation:** We discard the depth prediction module and exclude depth-related inputs entirely.
- **w/o Depth Estimation & Panoptic Segmentation:** Both depth estimation and panoptic segmentation are removed, leaving only RGB-based reasoning.

As shown in Table 3, each component contributes meaningfully to the model’s overall performance. Removing either the segmentation or the depth branch causes noticeable degradation, while removing both leads to the most significant performance drop. Notably, reconstructing a point cloud from depth provides additional spatial cues beyond raw depth values, validating the importance of 3D geometric understanding in complex OR scenes.

Conclusion

In this work, we present Spatial-ORMLLM, a novel multi-modal large language model tailored for 3D spatial reasoning in complex surgical environments using only RGB images. To overcome the limitations of modality-scarce clinical settings, our approach introduces a lightweight and extensible framework that generates three pseudo-modalities: depth maps, panoptic segmentation, and point clouds via a 3D Spatial Block. These modality-specific representations are projected into a unified token space and integrated through a spatial-enhanced fusion block, enabling the model to perform attention-based reasoning over semantic and geometric cues.

Comprehensive experiments on a dataset combined from MM-OR and 4D-OR demonstrate that our model achieves state-of-the-art performance on spatial reasoning and scene graph generation tasks, outperforming existing 2D and 3D vision-language baselines across all metrics. Our results validate that even under RGB-only input constraints, precise and structured 3D spatial reasoning is achievable. This highlights the potential of spatially grounded large language models for practical deployment in real-world clinical environments, paving the way for safer and more intelligent surgical assistance systems.

References

- Alayrac, J.-B.; Donahue, J.; Luc, P.; Miech, A.; Barr, I.; Hasson, Y.; Lenc, K.; Mensch, A.; Millican, K.; Reynolds, M.; Ring, R.; Rutherford, E.; Cabi, S.; Han, T.; Gong, Z.; Samangooei, S.; Monteiro, M.; Menick, J.; Borgeaud, S.; Brock, A.; Nematzadeh, A.; Sharifzadeh, S.; Binkowski, M.; Barreira, R.; Vinyals, O.; Zisserman, A.; and Simonyan, K. 2022. Flamingo: a Visual Language Model for Few-Shot Learning. In *Proceedings of Neural Information Processing Systems (NeurIPS)*.
- Chen, B.; Xu, Z.; Kirmani, S.; Ichter, B.; Sadigh, D.; Guibas, L.; and Xia, F. 2024a. SpatialVLM: Endowing Vision-Language Models with Spatial Reasoning Capabilities. In *Proceedings of the IEEE/CVF Conference on Computer Vision and Pattern Recognition (CVPR)*, 14455–14465.
- Chen, S.; Chen, X.; Zhang, C.; Li, M.; Yu, G.; Fei, H.; Zhu, H.; Fan, J.; and Chen, T. 2024b. LL3DA: Visual Interactive Instruction Tuning for Omni-3D Understanding Reasoning and Planning. In *Proceedings of the IEEE/CVF Conference on Computer Vision and Pattern Recognition (CVPR)*, 26428–26438.
- Chen, Z.; Gholami, A.; Nießner, M.; and Chang, A. X. 2021. Scan2Cap: Context-aware Dense Captioning in RGB-D Scans. In *Proceedings of the IEEE/CVF Conference on Computer Vision and Pattern Recognition*, 3193–3203.
- Deng, J.; He, T.; Jiang, L.; Wang, T.; Dayoub, F.; and Reid, I. 2025. 3D-LLaVA: Towards Generalist 3D LMMs with Omni Superpoint Transformer. In *Proceedings of the IEEE/CVF Conference on Computer Vision and Pattern Recognition*.
- Fan, Z.; Zhang, J.; Li, R.; Zhang, J.; Chen, R.; Hu, H.; Wang, K.; Qu, H.; Wang, D.; Yan, Z.; Xu, H.; Theiss, J.; Chen, T.; Li, J.; Tu, Z.; Wang, Z.; and Ranjan, R. 2025. VLM-3R: Vision-Language Models Augmented with Instruction-Aligned 3D Reconstruction. arXiv:2505.20279.
- Guo, D.; Lin, M.; Pei, J.; Tang, H.; Jin, Y.; and Heng, P.-A. 2024. Tri-modal Confluence with Temporal Dynamics for Scene Graph Generation in Operating Rooms. In *MICCAI*. Springer.
- Hong, Y.; Zhen, H.; Chen, P.; Zheng, S.; Du, Y.; Chen, Z.; and Gan, C. 2023. 3D-LLM: Injecting the 3D World into Large Language Models. *NeurIPS*.
- Huang, H.; Chen, Y.; Wang, Z.; Huang, R.; Xu, R.; Wang, T.; Liu, L.; Cheng, X.; Zhao, Y.; Pang, J.; et al. 2024a. Chat-scene: Bridging 3d scene and large language models with object identifiers. *Proceedings of the Advances in Neural Information Processing Systems, Vancouver, BC, Canada*.
- Huang, J.; Yong, S.; Ma, X.; Linghu, X.; Li, P.; Wang, Y.; Li, Q.; Zhu, S.-C.; Jia, B.; and Huang, S. 2024b. An Embodied Generalist Agent in 3D World. In *Proceedings of the International Conference on Machine Learning (ICML)*.
- Kamtam, D. N.; Shrager, J. B.; Malla, S. D.; Wang, X.; Lin, N.; Cardona, J. J.; Yeung-Levy, S.; and Hu, C. 2025. SurgiSAM2: Fine-tuning a foundational model for surgical video anatomy segmentation and detection. arXiv:2503.03942.
- Kirillov, A.; Mintun, E.; Ravi, N.; Mao, H.; Rolland, C.; Gustafson, L.; Xiao, T.; Whitehead, S.; Berg, A. C.; Lo, W.-Y.; Dollár, P.; and Girshick, R. 2023. Segment Anything. arXiv:2304.02643.
- Li, B.; Zhang, Y.; Guo, D.; Zhang, R.; Li, F.; Zhang, H.; Zhang, K.; Li, Y.; Liu, Z.; and Li, C. 2024. LLaVA-OneVision: Easy Visual Task Transfer. arXiv preprint arXiv:2408.03326.
- Li, J.; Li, D.; Savarese, S.; and Hoi, S. 2023. BLIP-2: Bootstrapping Language-Image Pre-training with Frozen Image Encoders and Large Language Models. In *ICML*.
- Liu, H.; Li, C.; Wu, Q.; and Lee, Y. J. 2023. Visual Instruction Tuning.
- Lou, A.; Li, Y.; Zhang, Y.; and Noble, J. 2024. Surgical Depth Anything: Depth Estimation for Surgical Scenes using Foundation Models. arXiv:2410.07434.
- Ma, W.; Ye, L.; de Melo, C.; Yuille, A. L.; and Chen, J. 2025. SpatialLLM: A Compound 3D-Informed Design towards Spatially-Intelligent Large Multimodal Models. In *Proceedings of the IEEE/CVF conference on computer vision and pattern recognition*.
- Qi, C. R.; Yi, L.; Su, H.; and Guibas, L. J. 2017. PointNet++: deep hierarchical feature learning on point sets in a metric space. In *Proceedings of the 31st International Conference on Neural Information Processing Systems, NIPS'17*, 5105–5114. Curran Associates Inc. ISBN 9781510860964.
- Radford, A.; Kim, J. W.; Hallacy, C.; Ramesh, A.; Goh, G.; Agarwal, S.; Sastry, G.; Askell, A.; Mishkin, P.; Clark, J.; Krueger, G.; and Sutskever, I. 2021. Learning transferable visual models from natural language supervision. *International Conference on Machine Learning (ICML)*.
- Wu, D.; Liu, F.; Hung, Y.-H.; and Duan, Y. 2025. Spatial-MLLM: Boosting MLLM Capabilities in Visual-based Spatial Intelligence. arXiv preprint arXiv:2505.23747.
- Yang, L.; Kang, B.; Huang, Z.; Zhao, Z.; Xu, X.; Feng, J.; and Zhao, H. 2024. Depth Anything V2. In *NeurIPS*.
- Zheng, L.; Chiang, W.-L.; Sheng, Y.; Zhuang, S.; Wu, Z.; Zhuang, Y.; Lin, Z.; Li, Z.; Li, D.; Xing, E. P.; Zhang, H.; Gonzalez, J. E.; and Stoica, I. 2023. Judging LLM-as-a-judge with MT-Bench and Chatbot Arena. arXiv:2306.05685.
- Zhi, H.; Chen, P.; Li, J.; Ma, S.; Sun, X.; Xiang, T.; Lei, Y.; Tan, M.; and Gan, C. 2025. LSceneLLM: Enhancing Large 3D Scene Understanding Using Adaptive Visual Preferences. In *Proceedings of the IEEE/CVF Conference on*

Computer Vision and Pattern Recognition (CVPR), 3761–3771.

Zhu, C.; Wang, T.; Zhang, W.; Pang, J.; and Liu, X. 2025. LLaVA-3D: A Simple yet Effective Pathway to Empowering LMMs with 3D-awareness. *ICCV*.

Zhu, Z.; Ma, X.; Chen, Y.; Deng, Z.; Huang, S.; and Li, Q. 2023. 3D-VisTA: Pre-trained Transformer for 3D Vision and Text Alignment. *ICCV*.

Özsoy, E.; Czempiel, T.; Holm, F.; Pellegrini, C.; and Navab, N. 2023. LABRAD-OR: Lightweight Memory Scene Graphs for Accurate Bimodal Reasoning in Dynamic Operating Rooms. In *International Conference on Medical Image Computing and Computer-Assisted Intervention*. Springer.

Özsoy, E.; Pellegrini, C.; Czempiel, T.; Tristram, F.; Yuan, K.; Bani-Harouni, D.; Eck, U.; Busam, B.; Keicher, M.; and Navab, N. 2025. MM-OR: A Large Multimodal Operating Room Dataset for Semantic Understanding of High Intensity Surgical Environments. In *CVPR*. Accepted.

Özsoy, E.; Pellegrini, C.; Keicher, M.; and Navab, N. 2024. ORacle: Large Vision-Language Models for Knowledge-Guided Holistic OR Domain Modeling. In *International Conference on Medical Image Computing and Computer-Assisted Intervention*, 455–465. Springer.

Özsoy, E.; Örmek, E. P.; Eck, U.; Czempiel, T.; Tombari, F.; and Navab, N. 2022. 4D-OR: Semantic Scene Graphs for OR Domain Modeling. In *International Conference on Medical Image Computing and Computer-Assisted Intervention*. Springer.

Spatial-ORMLLM: Improve Spatial Relation Understanding in the Operating Room with Multimodal Large Language Model

Appendix

Code and Dataset

Implementation and Code

We implement Spatial-ORMLLM using PyTorch, building on the open-source LLaVA codebase for multimodal LLM training. The vision-language architecture and training pipeline are modular, facilitating easy addition of new modalities. All model weights (including the 3D Spatial Block and Vicuna LLM) are initialized from pre-trained sources as described below. We will release our code and trained models to support reproducibility.

Data Preprocessing for MM-OR and 4D-OR

We consolidate the MM-OR and 4D-OR operating room datasets (totaling 46,742 samples) and apply a weakly-supervised preprocessing pipeline to enrich their annotations. Each raw data sample consists of multi-view RGB video frames (synchronized views of the same surgical scene) with associated depth sensor readings (e.g., Kinect), panoptic segmentation labels, and semantic scene graphs provided by clinical experts.

We treat each individual camera frame as a separate training sample for our model (i.e., each RGB image forms one sample). For each image, we derive three “pseudo-modal” annotations: a monocular depth map, a panoptic segmentation mask, and a 3D point cloud. These serve as additional visual inputs during model training. Crucially, we leverage the ground-truth depth and segmentation information in the datasets as weak supervision to fine-tune foundation models for depth estimation and segmentation. These fine-tuned models are then used to infer pseudo-modalities across all images. While ground-truth sensor data is available in the dataset, we do not feed it directly into the model; instead, we simulate an RGB-only inference scenario where all 3D cues are internally predicted.

Modality Filtering and Selection

The MM-OR and 4D-OR datasets contain additional modalities (e.g., audio, robot kinematics, instrument tracking logs), which are beyond the scope of our current vision-language modeling objectives. We filter out these modalities and focus on visual and semantic inputs. Specifically, we use RGB images and associated visual annotations (depth and segmentation) for inputs, along with textual annotations (scene descriptions and QA pairs) for outputs.

To reduce redundancy, we downsample frame rates and select representative keyframes from each surgical video. For multi-view data, we either designate a single primary view or treat each view independently, ensuring training samples are diverse in scene layout but restricted to a single RGB image plus internally generated pseudo-modalities.

Scene Graph Augmentation via LLM

Both OR datasets provide expert-annotated scene graphs describing objects (e.g., surgical staff, tools, patient, furniture) and their pairwise relations (e.g., “surgeon next to patient”, “nurse holding tray”). However, these graphs may be sparse or incomplete due to annotation costs and visual ambiguity.

We employ GPT-4 to augment and convert these structured annotations into detailed natural language descriptions for LLM training. Given a list of detected entities and relations (graph triples) and relevant context (e.g., surgical phase), we prompt GPT-4 to generate coherent scene paragraphs. These generated captions serve as ground-truth targets for our vision-language learning, expanding supervision beyond limited human-authored data.

Additionally, we use GPT-4 to propose plausible but implicit relations. For example, if a graph contains “surgeon beside table” and “nurse beside table”, GPT-4 may infer “surgeon opposite nurse”. These extra triples are added as weak supervision without manual verification (except for spot checks), allowing scalable expansion of training data.

Usage for RGB-Only vs. Full-Modal Tasks

Our processed dataset supports two evaluation modes: (1) *RGB-only*, where the model receives only raw images and must infer 3D understanding internally; and (2) *full multimodal*, where the model utilizes the entire pipeline of inferred depth, segmentation, and point cloud features.

In practice, Spatial-ORMLLM always enables pseudo-modal reasoning. Even under “RGB-only” settings, the model internally predicts depth and segmentation from the RGB image. However, to fairly compare against baselines lacking 3D enhancements (e.g., ORacle, MM2SG), we evaluate some tasks under a strict RGB-only regime by restricting external inputs to raw images. For instance, in scene graph generation, all models are fed only RGB images. While our model still uses its internal pseudo-modal estimation, baselines rely solely on 2D input.

In contrast, for primary spatial reasoning tasks (e.g., descriptive QA), we utilize full pseudo-modal input: RGB images enriched with model-generated depth, segmentation, and point cloud tokens. At no point is ground-truth 3D sensor data used during inference. The distinction lies solely in whether internal pseudo-modal features are allowed to guide the reasoning process—enabled for our model, but disabled for 2D-only baselines during ablations.

Implementation Details

Hyperparameter Selection

We performed extensive hyperparameter exploration to finalize our training configuration.

In Stage 1 (language-only pre-training), we fine-tuned the Vicuna-v1.5-7B language model on surgical domain instructions using a learning rate of 2×10^{-5} and the AdamW optimizer (with $\beta_1=0.9$, $\beta_2=0.999$). We experimented with learning rates in $\{1 \times 10^{-5}, 2 \times 10^{-5}, 5 \times 10^{-5}\}$ on a held-out set of medical Q&A pairs, observing that 2×10^{-5} yielded the best stability and lowest perplexity. A smaller learning rate led to underfitting domain-specific terms, while a higher rate sometimes degraded the fluent tone of the pre-trained LLM. We trained Stage 1 for 10 epochs on a corpus of approximately 3k curated instruction-following examples (see below), using a batch size of 64, linear learning rate warmup over 500 steps, and cosine decay.

In Stage 2 (vision-language fine-tuning), we freeze the LLM and tune only visual modules, which allows for a larger learning rate without destabilizing language generation. We conducted a grid search over $\{5 \times 10^{-4}, 1 \times 10^{-3}, 2 \times 10^{-3}\}$ for the vision learning rate and found that 1×10^{-3} was optimal for fast convergence. All projection heads and newly introduced layers used this learning rate, while pretrained image encoders (e.g., CLIP ViT and the depth/segmentation backbones) were fine-tuned at a slightly lower rate (5×10^{-4}) to preserve their pretrained features. We applied separate AdamW optimizers for these parameter groups.

The effective batch size was set to 128 (synchronizing gradients across 8 GPUs) based on memory and stability considerations.

We also explored various loss weightings: the language modeling loss versus contrastive loss ratio λ was swept in $\{0.05, 0.1, 0.2\}$. Ultimately, $\lambda=0.1$ (i.e., a 10:1 weighting favoring LM loss) gave the best validation performance.

Other hyperparameters such as dropout (0.1), weight decay (0.01), and warmup steps (500) were kept consistent with LLaVA settings or the original Vicuna training recipe.

Table A1 summarizes the key hyperparameters and the range of values tried; we selected the final values based on the highest validation CIDEr score for spatial question answering.

Hyperparameter	Value
Language LR (Stage 1)	2e-5
Vision LR (Stage 2)	1e-3
Pretrained Vision LR	5e-4
Effective Batch Size	128
Optimizer	AdamW
Adam β_1, β_2	0.9, 0.999
LR Warmup Steps	500
LR Decay	Cosine
LM vs. Contrastive Loss λ	0.1
Dropout	0.1
Weight Decay	0.01
Epochs (Stage 1)	10
Epochs (Stage 2)	10

Table A1: Final hyperparameter settings used in our two-stage training.

Training Procedure and Strategy

We adopt a two-stage training strategy, as outlined in the main paper.

Stage 1: Language Reasoning Adaptation. We aim to inject domain knowledge into the LLM. To this end, we construct a curated dataset of instruction–response pairs related to operating room scenarios. Examples are synthesized using GPT-4 and then lightly edited. We fine-tune the Vicuna-7B model using this corpus in a supervised, text-only setting, with all visual modules frozen. The loss function is the standard causal language modeling loss over the reference answer tokens:

$$\mathcal{L}_{\text{LM}} = - \sum_{t=1}^T \log P(y_t | y_{<t}, x) \quad (13)$$

where x is the input prompt, and y_1, \dots, y_T are the ground-truth response tokens.

Training lasts for 10 epochs, after which the LLM demonstrates robust use of medical terminology and spatial expressions (e.g., correctly interpreting “across the table”).

Stage 2: Visual Alignment and Fusion Tuning. In this stage, we freeze the Vicuna LLM and fine-tune the visual frontend. This includes the CLIP ViT-L/14 image encoder, the depth and segmentation backbones (VFM module), and all modality-specific projection heads. We use the previously described preprocessed multimodal supervision dataset, consisting of RGB images paired with textual scene annotations.

To align image and text features, we use a composite loss:

$$\mathcal{L}_{\text{Stage2}} = \mathcal{L}_{\text{LM}} + \lambda_{\text{CLIP}} \cdot \mathcal{L}_{\text{contrast}} \quad (14)$$

Here, λ_{CLIP} controls the relative weight of the contrastive loss. We set $\lambda_{\text{CLIP}} = 0.1$ based on validation performance.

Following LLaVA, the contrastive loss aligns global image and text features. Specifically, we extract the projected $[CLS]$ token \mathbf{v}_i from the image encoder and the $[SOS]$ token \mathbf{t}_i from the LLM for each sample i . The contrastive loss over a batch of N samples is defined using InfoNCE:

$$\mathcal{L}_{\text{contrast}} = - \frac{1}{N} \sum_{i=1}^N \log \frac{\exp(\text{sim}(\mathbf{v}_i, \mathbf{t}_i)/\tau)}{\sum_{j=1}^N \exp(\text{sim}(\mathbf{v}_i, \mathbf{t}_j)/\tau)} \quad (15)$$

where $\text{sim}(\cdot, \cdot)$ denotes cosine similarity, and τ is a temperature hyperparameter (set to 0.07 by default).

This formulation encourages matched image-text pairs $(\mathbf{v}_i, \mathbf{t}_i)$ to have higher similarity than mismatched ones $(\mathbf{v}_i, \mathbf{t}_j)$, promoting consistent cross-modal alignment.

We train Stage 2 for 10 epochs over 46k samples. The final checkpoint is selected based on average performance on a held-out validation set, using ROUGE-L, METEOR, CIDEr, and EM metrics. All training is conducted on 8 NVIDIA A100 GPUs. We did not observe overfitting due to the diversity of the training set and did not apply early stopping.

3D OR Understanding via MLLM

Visual Feature Modulator (VFM)

The Visual Feature Modulator is implemented as a dual-branch encoder–decoder network that generates a depth map $D \in \mathbf{R}^{H \times W}$ and a panoptic segmentation map $S \in \{1, \dots, K\}^{H \times W}$ from an input image $I \in \mathbf{R}^{3 \times H \times W}$.

Shared Encoder The input image is processed by a shared encoder composed of 12 transformer blocks, yielding a compact latent representation:

$$F_{\text{enc}} = E_{\text{VFM}}(I), \quad F_{\text{enc}} \in \mathbf{R}^{C \times H' \times W'} \quad (16)$$

where $C = 768$, and H', W' denote reduced spatial dimensions.

Depth Decoder The depth decoder is a 4-stage upsampling module that progressively refines the geometric features via bilinear interpolation, convolution, and skip connections. The output depth map is obtained as:

$$D = D_{\text{depth}}(F_{\text{enc}}), \quad D \in \mathbf{R}^{H \times W} \quad (17)$$

Each stage of the decoder consists of:

$$F^{(i)} = \text{Conv}_{3 \times 3}(\text{Up}(F^{(i+1)})) + \text{Skip}(F_{\text{enc}}^{(i)}) \quad (18)$$

for $i = 3, 2, 1, 0$, where $\text{Up}(\cdot)$ denotes bilinear upsampling, and $F_{\text{enc}}^{(i)}$ is the corresponding encoder feature from the same scale.

Segmentation Decoder The segmentation decoder adopts a similar upsampling structure and is equipped with transformer attention blocks to enhance semantic prediction. The final segmentation output is defined as:

$$S = D_{\text{seg}}(F_{\text{enc}}), \quad S \in \{1, \dots, K\}^{H \times W} \quad (19)$$

The intermediate segmentation logits are computed as:

$$Z_{\text{seg}} = \text{MLP}(\text{Up}^4(F_{\text{enc}})) \in \mathbf{R}^{K \times H \times W} \quad (20)$$

and the semantic prediction at each pixel is obtained by:

$$S(u, v) = \arg \max_k Z_{\text{seg}}[k, u, v] \quad (21)$$

Reasoning Decoder

Architecture and Input The Reasoning Decoder is a transformer-based module with $L = 6$ layers, hidden size $D = 768$, and 8 heads per layer. It takes as input the contextual embeddings from the LLM:

$$H = \text{LLM}([Q; T_{\text{fusion}}]) \in \mathbf{R}^{(M+N) \times D},$$

where Q is the sequence of question tokens and T_{fusion} are the fused multi-modal tokens.

Autoregressive Decoding Let $y_{<t}$ be the previously generated tokens. At decoding step t , the decoder computes:

$$P(y_t | y_{<t}, H) = \text{softmax}(W_o Z_t^{(L)}), \quad (22)$$

where $Z_t^{(L)}$ is the decoder hidden state at layer L , and $W_o \in \mathbf{R}^{D \times |\mathcal{V}|}$ is the output projection.

Loss and Inference The training objective is to minimize the negative log-likelihood:

$$\mathcal{L}_{\text{ans}} = -\frac{1}{T} \sum_{t=1}^T \log P(y_t^* | y_{<t}^*, H). \quad (23)$$

During inference, the decoder generates tokens autoregressively using beam search or greedy decoding.

OR-Specific Reasoning Capabilities The decoder generates spatially grounded responses (e.g., “The instrument table is to the right of the patient”), leveraging both segmentation-aware object identities and depth-derived spatial layouts. It handles surgical roles, equipment relations, and proximity reasoning in cluttered OR scenes.

Additional Experiments

More Visualization Examples

To further showcase Spatial-ORMLLM’s capabilities in spatial reasoning and attention to critical surgical entities, we present five additional qualitative examples in Figure A1. Each example corresponds to a representative operating room scene, visualized from three different viewpoints to reflect the multi-perspective nature of OR spatial understanding.

These visualizations highlight how our model interprets the relative positioning of staff and instruments, and selectively focuses on surgically relevant entities such as the patient, lead surgeon, instrument table, and anesthesia devices. The incorporation of depth and segmentation cues enables the model to distinguish foreground/background arrangements (e.g., “in front of the surgical bed”) and to disambiguate between visually similar entities occupying different spatial roles.

Compared to the main paper, which includes limited qualitative samples, Figure A1 offers a more comprehensive view of our model’s ability to generate detailed and spatially grounded scene descriptions under varying OR configurations.

More Downstream Task

Next-Action Prediction To assess the applicability of our model to clinically relevant downstream tasks, we evaluate it on the next-action prediction task from the MM-OR benchmark. Given an RGB image representing the current surgical state and a brief textual prompt, the model must predict the most likely next surgical action. This task emphasizes both spatial comprehension and procedural reasoning under visual constraints.

To ensure a fair comparison, we constrain all models to use RGB-only input. No temporal, depth, or segmentation information is available during inference, simulating a realistic setting where only standard surgical video is provided.

As shown in Table A3, our model achieves the highest performance with an F1 score of 36.8%, slightly surpassing the multimodal-trained MM2SG baseline, which reports 35.4% in the unconstrained setting but drops significantly to

The nurse is **draping** the patient **on** the operating table, while another nurse is preparing instruments **beside** the surgical area.

The surgeon is **drilling** the patient using the Mako robot, with the nurse **standing beside**. The circulator is operating the monitor **in the corner**.

One surgeon is operating the monitor **in the front-left corner** of the room, while another is adjusting the display **near the right** wall. Meanwhile, a nurse is cleaning the Mako robot positioned **centrally** in the operating area.

One nurse is preparing the Mako robot **beside** the cabinet wall, while another nurse is pulling the patient **on** the operating table **toward the center** of the OR.

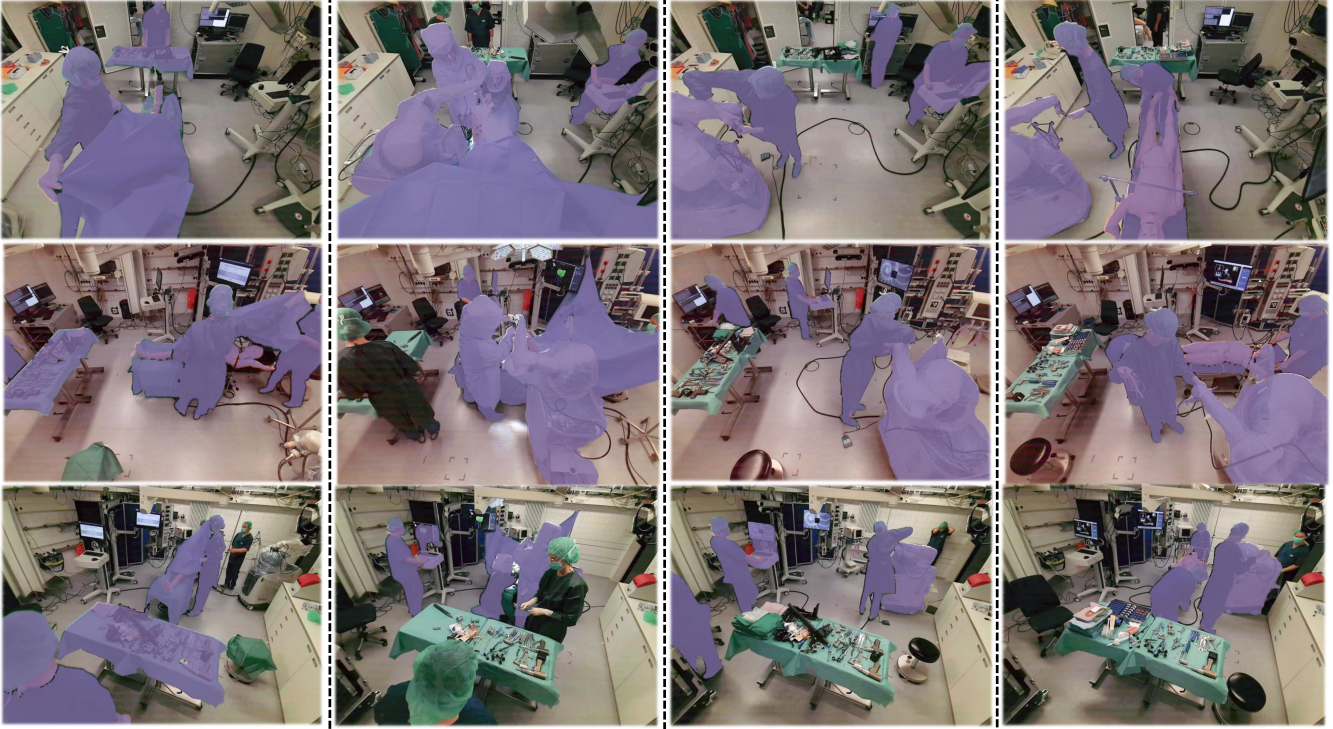


Figure A1: Qualitative visualization of Spatial-ORMLLM on four representative OR scenes, each shown from three view-points. The visualizations highlight the model’s ability to identify key surgical entities (e.g., patient, surgeon, operating table) and reason about their spatial relations. The integration of depth and segmentation pseudo-modalities enables fine-grained understanding of foreground-background structure and spatial configurations. These examples demonstrate our model’s consistent spatial awareness across diverse OR layouts and perspectives.

27.1% under RGB-only input. GPT-4V achieves a middle-ground performance of 32.0%, reflecting some general procedural awareness but lacking domain-specific grounding. These results validate the robustness of Spatial-ORMLLM’s spatial reasoning and suggest its strong generalization capability in constrained clinical environments.

Robot Phase Prediction To further assess the spatial-semantic reasoning capability of Spatial-ORMLLM in real-world robotic surgery, we evaluate it on the robot phase prediction task from the MM-OR benchmark. In this task, the model must infer the current surgical phase (e.g., “ablation”, “suturing”) based solely on the interpreted scene graph, simulating decision-making based on structured perception.

Following the official MM-OR protocol, we fine-tune a language-only decoder that receives as input the scene graph

tokens along with the task prompt “phase recognition”. To ensure a lightweight and controlled comparison, all models operate in RGB-only input.

Table A4 shows that our Spatial-ORMLLM model achieves an F1 score of 58.2%, outperforming the multi-modal MM2SG baseline, which reports 56.9% in the unconstrained setting but drops significantly to 49.3% under RGB-only input. GPT-4V, which generalizes across domains but lacks OR-specific fusion, obtains 54.0%. These results demonstrate Spatial-ORMLLM’s robust ability to encode surgical state representations even under partial modality inputs.

Additional Ablation Studies

To further validate the design of Spatial-ORMLLM’s fusion strategy, we conduct two additional ablation studies that ex-

Model Variant	R-L(%) \uparrow	M(%) \uparrow	C \uparrow	EM(%) \uparrow	AVG \uparrow	P(%) \uparrow	R(%) \uparrow	F1(%) \uparrow
w/o Spatial-Enhanced Fusion Block	56.4	50.6	88.3	59.1	63.6	83.0	80.1	81.5
Depth & Seg as Stacked Input	59.2	53.3	91.0	63.2	66.7	85.2	82.0	83.5
Spatial-ORMLLM (Full)	61.2	58.6	96.4	67.8	71.0	86.1	83.3	84.7

Table A2: Ablation results for different visual fusion strategies in Spatial-ORMLLM. The first five metrics (ROUGE-L, METEOR, CIDEr, EM@1, AVG) evaluate spatial reasoning, while the last three (Precision, Recall, F1) evaluate scene graph generation.

Model	F1 Score (%)
MM2SG (RGB-only)	27.1
GPT-4V	32.0
Spatial-ORMLLM (Ours)	36.8

Table A3: Next-Action Prediction on MM-OR. F1 score (%) for predicting upcoming surgical actions from RGB frames.

Model	F1 Score (%)
MM2SG (RGB-only)	49.3
GPT-4V	54.0
Spatial-ORMLLM (Ours)	58.2

Table A4: Robot Phase Prediction on MM-OR. F1 score (%) for recognizing the current robot phase based on generated scene graphs.

explore alternative methods for integrating the depth and segmentation pseudo-modalities. Importantly, both variants retain access to all input signals (RGB, depth, and segmentation), but differ from our full model in how these modalities are fused.

(1) Without Spatial-Enhanced Fusion Block. This variant removes the dedicated token-level fusion mechanism. Instead of projecting each modality into a distinct token stream, we apply an early fusion approach: the depth map is appended as an extra image channel, and the segmentation mask is recolored and overlaid on the RGB input. The resulting composite image is passed into a single vision encoder without any modality-specific projections. This simplification tests whether our spatial-aware fusion architecture is truly necessary or if the model can learn sufficient multimodal features from raw pixel-level integration alone.

(2) Depth & Segmentation as Stacked Input. Here, we simulate a model that treats depth and segmentation as parallel views. Each modality (RGB, depth, segmentation) is encoded by a shared-weight vision tower independently, and their features are concatenated at a later stage. Unlike our method, which provides tokenized and semantically specialized representations for each modality, this approach relies on the visual encoder to jointly learn meaningful fusion from the stacked feature set. It serves as a middle ground between naive early fusion and our token-level multimodal integration.

Table A2 reports results on both spatial reasoning (evalu-

ated by ROUGE-L, METEOR, CIDEr, EM@1, and average QA score) and scene graph generation (evaluated by Precision, Recall, and F1). While both ablations yield reasonable performance, they lag behind the full Spatial-ORMLLM across all metrics. In particular, removing the spatial fusion block leads to a noticeable drop in F1 and average QA score, highlighting the importance of structured token-level integration. The stacked input variant performs slightly better, but still falls short compared to the full model.